La Metallurgia Italiana
International Journal of the Italian Association for Metallurgy

Quantification of Critical Parameters for Prediction of Surface Crack Formation in Continuous Casting

R. Krobath, C. Bernhard

One focus of the digitalization of the CC process is product quality prediction. The training of quality prediction modules can be achieved by experimental data. A requirement is the performance of experiments with samples simulating conditions close to the process. A challenging task is the forecast of surface cracks. At the Montanuniversitaet Leoben, a unique testing setup was developed, called the In-Situ Material Characterization by Bending (IMC-B) test. This test represents an experimental method, combining solidification, controlled cooling, and deformation in one sequence. It allows the prediction of surface crack formation with respect to the testing conditions. Varying testing parameters enable the determination of the impact of different factors that lead to crack formation during deformation of a casted sample in a 3-point bending test. As output quantification parameters for damage evaluation are provided by defining a critical strain for crack formation. This study shows the susceptibility to transverse crack formation of a low alloyed construction steel in the temperature range of the second ductility trough.

KEYWORDS: SURFACE CRACK FORMATION, IN-SITU BENDING TEST, TRANSVERSE CRACKS, ELASTO-VISCOPLASTIC MATERIAL MODEL, STRAIN ANALYSES, CRITICAL STRAIN;

NTRODUCTION

Virtual "copies" of the continuous casting machines, called digital twins, are constructs of dynamic and complex unions of specific calculation and monitoring modules [1]. Accurate data, generated by sophisticated experiments, are used in thermophysical models to calculate solidification and strand temperatures [2]. This also serves as the basis for product quality prediction, which can be done by specific implemented quality prediction modules. The goal of digital quality prediction is the forecast of a certain risk for problems under the predominating casting conditions. This is a very challenging task, especially for the surface quality. When focused on the surface crack formation, the process factors and parameters that influence the formation and finally lead to surface cracks are widely spread. This results in several possible types of surface cracks and defects, which are summarized in earlier publications [3-5].

Data for the adjustment and further development of surface quality prediction can be generated in the plant by product inspection and quality tracking. This approach has the advantage of a self-learning process. Still, it can

Roman Krobath
Montanuniversität Leoben, Austria

Christian Bernhard
Montanuniversität Leoben, Austria

especially be challenging in the CC process, as the surface quality influencing factors are widely spread, and the inspection of the semis is impeded due to environmental factors, such as high temperatures and scale on the product surface. When used as a single approach, there is the risk of overlooked influencing factors and misinterpretation of results. An additional method for the further development of quality prediction modules is to create data from experimental investigations with respect to the process. Therefore, requirements for the plausibility of provided data are experimental procedures under near-process conditions. If this is fulfilled, concerning selected topics, such experiments can be called "experimental twins". For the surface crack formation, an "experimental twin" should be able to simulate certain process parameters and material behavior close to process conditions. Especially when combined with the approach of product inspection, models can be tuned and validated.

Typical experiments characterizing the strand shell ductility are conventional hot ductility tests, usually performed as uniaxial hot tensile tests or compression and torsion tests. In consideration of the heat treatment and deformation parameters, reduction of area values can describe certain factors that influence the ductility, e.g., grain size, precipitations, and the austenite to ferrite transition. Process-near simulations with, e.g., coarse grain annealed microstructure or in-situ melted sample material and fluctuating cooling sequences bring sophisticated findings in the hot ductility of the strand shell [6-13].

Nevertheless, Crowther [14] concluded that due to the high strains to fracture in the tensile experiments, a bend test for the simulation of transverse crack formation should give an even more reliable indicator. Such experiments were already developed for reheated samples [15-17] and in-situ casted samples, improving the approach to process conditions [18, 19]. These experiments give promising results regarding the indication of surface crack formation.

This paper explains a bend test for investigating the susceptibility to surface crack formation, which is operated at the Montanuniversitaet Leoben, called the In-situ Material Characterization by Bending (IMC-B) test. It represents an experimental method combining solidification, controlled cooling, and defined deformation of samples in one testing sequence [20-22].

EXPERIMENTAL PART

Methodology

In the IMC-B test, every sample is cast separately in a steel mold where solidification and mold cooling occurs. The residual time in the mold is adjusted to the aim of the simulated process conditions. Fig. 1, left upper picture, depicts the workflow of the method, which is divided into 3 steps. The split construction of the mold allows fast and easy removal of the sample finishing step I of the test.

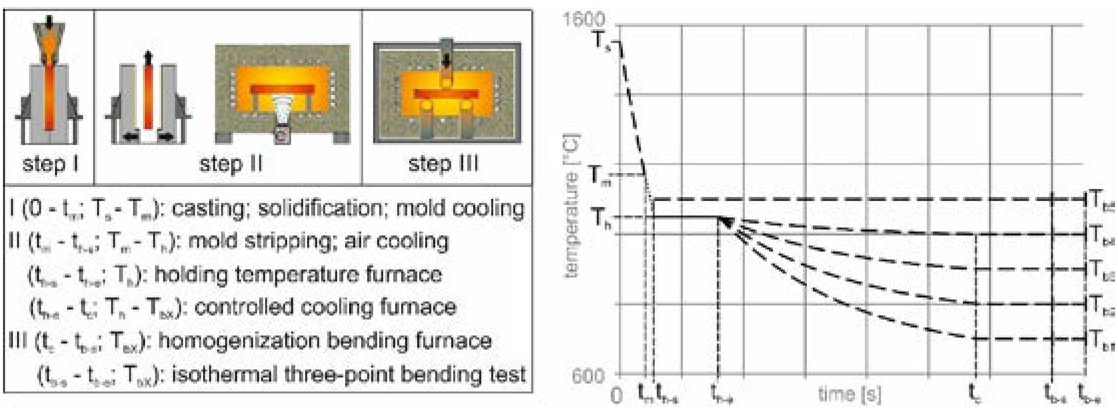

Fig.1 - Workflow of the IMC-B test and schematic cooling curves within the definition of significant points [22].

Continuing in step II, the sample is cooled down according to a specific thermal sequence reaching a defined target value, which represents the later on bending temperature. This is managed by a stepwise apposition of chamber furnaces with varying temperatures. During this thermal cycle, the sample surface temperature is continuously measured with an optical pyrometer. For bending, the sample is positioned in bending equipment on the bearing stamps, where the temperature field is homogenized at bending temperature. At a defined starting point, isothermal bending of the sample takes place, realized with the movement of the bending stamp. The well-controllable facility allows accurate bending parameters, either force or displacement controlled. This deformation of the sample should simulate local strand shell deformation, e.g., during bending and straightening. Finally, the sample is cooled to room temperature by smooth cooling to minimize the thermal and transition-induced stresses and strains or quenched in order to freeze the microstructure. Every sample is descaled, and the surface is investigated in detail with a digital microscope. The defects and cracks are documented with respect to their position on the sample surface.

Fig. 1 shows schematic temperature-time curves for the IMC-B test. The sequence is defined by significant points within the three main steps listed and explained on the left-hand side. When displacement controlled tests are performed, the deformation characteristics are given by stamp velocity and displacement. The velocity is constant during the loading and unloading stages. The material behavior during bending is simulated with the Finite Element (FE) software package Abaqus. The material model parameters are adjusted to the material behavior of the in-situ casted samples, which can be significantly different from reheated samples. The constitutive material model combines elastic, plastic, and viscoplastic effects, allows accurate analyses of the sample's stress and strain fields, and is explained by Krobath et al. in a recently published work [23]. Fig. 2 shows a draft of the FE model with the mesh and the significant control and evaluation points. A quarter of the sample with symmetry planes in x- and z-direction is used. The translational and rotational values of the bearing are fixed (control point "support"). Evaluation of the force and displacement takes place at the control point "punch". Two-dimensional evaluations of stresses and strains on the sample surface in the x-direction depending on the distance to the bending axis are displayed as mean values over the sample width.

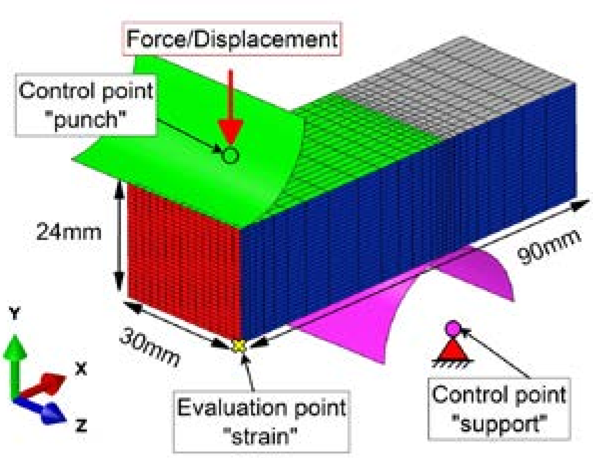

Fig.2 - FE model for simulating material behavior in the 3-point bending test [23].

A main characteristic of the IMC-B test is the usage of in-situ cast samples. The coatings enable controlled heat flux in the mold resulting in directional dendrite growth and associated coarsening of the dendrite and columnar grain structure, as shown in Fig. 3 b). Due to the well-controlled heat withdrawal, the resulting structure is similar to the structure of a strand shell surface; see Presslinger et al. [24] and Fig. 3 a). Metallographic investigations reveal the coarse columnar austenitic grain structure of IMC-B samples, depicted in Fig. 3 d) for a 0.17 wt.% C steel. The mean grain size depends mainly on the heat withdrawal in the mold and can therefore also be adjusted to the grain size at the slab surface, as shown by Reiter et al. [25]. The steel composition also plays an important role in the appearance of the austenite grain structure in directional solidification. Ohno et al. [26] show these correlations with samples investigated with rapid directional solidification equipment. A typical coarse columnar austenite grain structure for plain carbon steels in the range of 0.1 to 0.2 wt.% C is shown in Fig. 3 c). IMC-B-tests may be performed either after controlled cooling in air or protection by inert gas, such as Ar. Usually, the bending tests are performed after cooling in air. This results in strong oxidation of the surface but also, depending on the steel composition and here namely the content of certain elements like Si, Al and Mn, in intergranular and inner oxidation. A recent study by Krobath et al. [22] shows the harmful impact of a certain stronger intergranular oxidation on the formation of surface cracks in the bending experiments. It points at a possible strong influence of oxidation reactions of the sample surface with respect to tested conditions and composition. It makes the results of the bending experiment dependent on the cooling conditions. If this effect should be suppressed, the sample may also be shielded by inert gases during cooling and surface oxidation is mostly prevented.

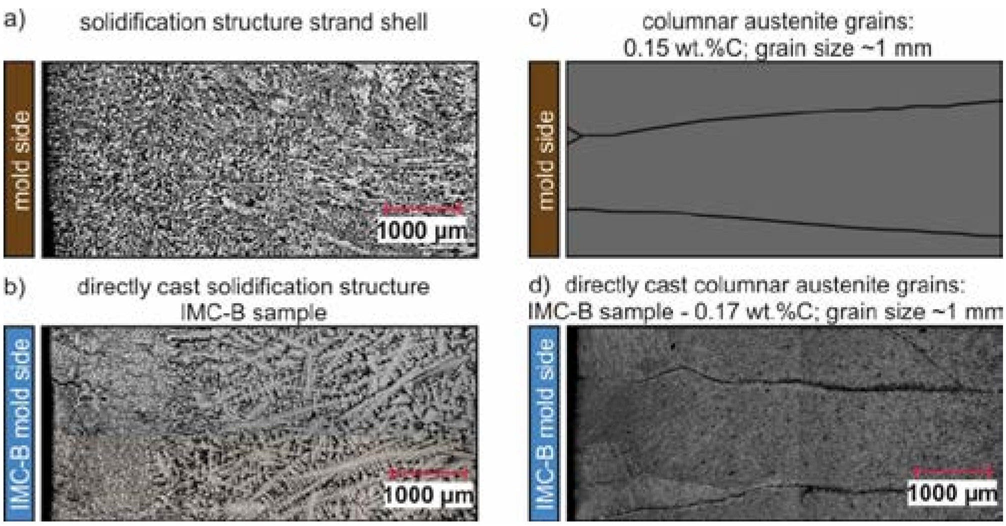

Fig.3 - Comparison of microstructures: a) Solidification structure strand shell; b) Solidification structure IMC-B sample; c) Coarse columnar austenite grains (scheme) [26]; d) Typical coarse columnar austenite grains in IMC-B sample - 0.17 wt.% C steel.

Testing Parameters

The basic composition for the following results is listed in Tab. 1. It represents an Al deoxidized 0.17 wt.% C construction steel. The significant points for the temperature sequence are shown in Tab. 2.

Tab.1 - Basic steel composition - all values in wt.%.

STEEL COMPOSITION						
C	Si	Mn	P	S	Al	N
0.17	0.4	1.55	0.01	<0.004	0.03	<0.008

Tab.2 - Significant points in the temperature sequence.

TEMPERATURE SEQUENCE					
t_m [s]	T_m [°C]	T_h [°C]	t_{h-e} [s]	t_{b-s} [s]	T_{bX} [°C]
45	~1180	1050	160	700	700-1100

The liquid steel is poured into the mold with a starting temperature of ~1550°C. The time of 45 s in the mold results in a surface temperature of ~1180°C afterwards.
The holding temperature T_h is 1050°C (except for samples with a bending temperature T_b of 1100°C) and the total time at the start of bending is 700 s. It is related to the start of the straightening process of a slab caster with a casting speed of 1.2 m/min and a slab thickness of 225 mm; see Krajewski et al. [27].
T_b ranges between 700°C and 1100°C in 50°C steps. The testing sequence is done in air atmosphere. After the bending test, each sample is cooled to room temperature with mild cooling rates between ~5 °C/min to ~1 °C/min, depending on the value of T_b. The bending stamp velocity for the loading and unloading step is 0.04 mm/s. Stamp displacements of 3 mm and 5 mm are applied for the whole temperature range.
Tests get reproduced at T_b = 850°C and T_b = 1050°C. Stamp displacements of 2 mm, 3 mm, 4 mm and 5 mm are tested at the bending temperature of 900°C. For the validity of reproduction, in this case every test is performed twice.

RESULTS
Simulation
The displacement of the stamp triggers the induced maximum strain and the strain distribution on the sample. Conventional IMC-B tests are performed with maximum displacements up to 5 mm. An advantage of the three-point bending test is an induced strain distribution on the sample surface. This enables the investigation of the impact of strains from 0 to a maximum strain on the formation of cracks with respect to the distance from the bending axis in a certain range of strain rates. Fig. 4 a) depicts the total strain distributions in the x-direction (LE11) for two cases of stamp displacement and resulting maximum strains at T_b = 900°C, displacement = 3 mm - max. strain = 3.5% and displacement = 5 mm - max. strain = 5.9%. It illustrates that the higher deflection results in a higher maximum strain, but it also covers the strain ranges of the sample with a lower deflection. A total displacement of 5 mm leads to maximum strains in the x-direction of between 5.9% (T_b = 900°C) and 6.4% (T_b = 1000°C) for the investigated temperature range. Differences in the strain distributions with same displacements are according to changes in the material behavior between the bending temperatures.

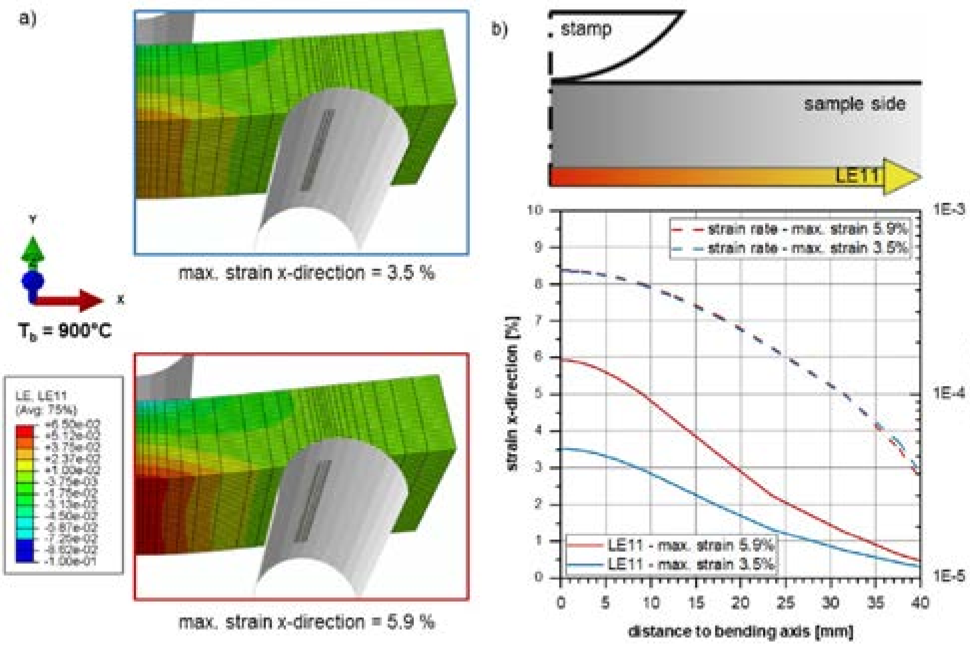

Fig.4 - a) Strain distributions at T_b = 900°C; max. strain in bending axis 3.5% (displacement = 3 mm) and max. strain in bending axis 5.9% (displacement = 5 mm); b) Mean strain values in x-direction and the corresponding strain rates against the distance to the bending axis corresponding to the bending cases in a).

The detailed strain evaluations of the two bending cases are visualized in Fig. 4 a) are shown in the diagram in Fig. 4 b). It contains the mean strain values in x-direction and the corresponding strain rates against the distance to the bending axis. The strain rates coincide nearly fully within values of $3 \cdot 10^{-5}$ s^{-1} to $4.7 \cdot 10^{-4}$ s^{-1}. The values correlate to surface strain rates during straightening in continuous casting, which are calculated to be in the range of max. ~$4 \cdot 10^{-4}$ s^{-1} to max. ~$6 \cdot 10^{-5}$ s^{-1}, with respect to machine parameters [28]. In contrast, the gap between the strains gets higher with decreasing distance to the bending axis. At an interval of 40 mm, the strains of both cases are still below 0.5%. The test with a higher deflection reaches 2% surface strain at ~25 mm distance. For the test with lower deflection, it is obtained at 17.5 mm. This strain is known as the guide value for maximum mechanically induced strains during straightening [3,14]. As the value can shift, e.g. due to thermal strains and higher strains in the case of notch effects in oscillation marks or surface pores [29], the higher strains are also considered for interpretation. The diagram expresses the advantage that positions of documented cracks can be directly related to a certain induced strain.

Surface Crack Investigation

Every sample surface is analyzed in detail. The defects must be carefully investigated, as the morphology can obtain information about the temperature zone where they formed. Cracks with paths through the bulk of austenite grains and fully dendritic morphology indicate defects formed in the first ductility trough during solidification. The triggers are remaining liquid phases at the liquid-solid interface, enriched with segregated elements and a lower melting point. Initialized strains are concentrated at these phases, resulting in the formation of pores growing to cracks with increasing strain. The temperature range reaches from solidus to the "zero ductility temperature" ~50°C below solidus [30, 31]. To evaluate the ductility in the area of 700°C to 1100°C, these defects cannot be considered. Nonetheless, they provide information concerning the behavior during solidification in the mold. Cracks formed due to the bending of the sample are intergranular (IG) at the austenite grain boundaries and range from ~50 μm to ~3 mm in length. Fig. 5 shows different crack arrangements. Fig. 5 a) depicts a typical singular crack and b) crack clusters. Singular IG cracks are the most frequently observed crack type. The crack clusters are areas with many orientated cracks in which a separation of the singular cracks is already difficult. They often form when a very critical state is simulated in samples with a substantial number of cracks. Network cracks, shown in Fig. 5 c), are unoriented cracks that can form on samples where pre-defects such as intergranular high temperature oxidation takes place [23].

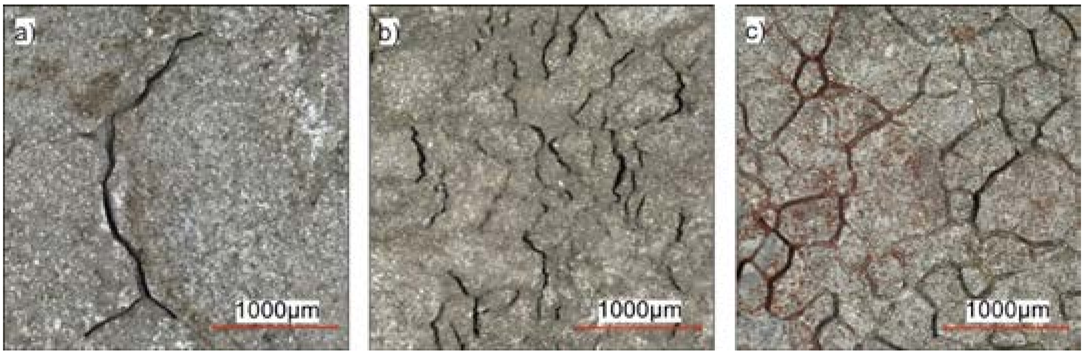

Fig.5 - a) Singular orientated IG cracks; b) Crack clusters; c) Network cracks.

Quantification Parameters

The first quantification parameter of the crack formation is the total number of cracks. It indicates the surface damage due to the bending test, taking into account all testing parameters, including the bending case. Fig. 6 a) shows the results for the described testing parameters and the two bending cases in Fig. 4. The labeled explanation shows the max. strain mean value for the investigated temperature range of 700°C to 1100°C. At 3.6% the four bending temperatures between 850° and 1000°C show a number of IG cracks between 18 and 28. All other remaining samples revealed no IG cracks at the sample surface (except one crack at 800°C). The test at 850°C was successfully reproduced with values of 18 and 22. The temperatures where no cracks formed can be described as not critical, but because of the only minor differences in the number of cracks at the other temperatures, no clear statement as to which temperature is the most critical is possible for this deflection. In comparison, the higher strains lead to significantly higher gaps. The samples in the lower temperature range of 700°C to 750°C still show no cracks. This leads to the first conclusion that this steel reveals no susceptibility to surface cracking at these temperatures with the current testing sequence. 37 cracks are documented for a bending temperature of 800°C. The high temperatures 1050°C and 1100°C show 59 and 11 cracks, respectively. A second sample at 1050°C with 64 cracks shows a similar result. The most critical temperatures are also found to be between 850°C and 1000°C. But for the higher stains, a considerable deterioration from 113 (1000°C) to 229 (850°C) cracks is identified. Fig. 7 shows the corresponding crack distributions at the surfaces. The mesh indicates the crack positions and the crack density 40 mm left and right of the bending axis in the temperature range of 800°C to 1000°C. Categories for segments visualize the crack distributions. White means no cracks, yellow means 1 to 5 cracks and red means more than 5 cracks. The highest crack density is clearly visible for the sample bent at 850°C with the higher maximum strain.

Within the total number of cracks, noncritical temperatures and temperatures with significantly more cracks can be explained. To reach a quantified appraisal of the crack formation regarding continuous casting, a critical strain for first crack formation is established. According to the crack positions and the development of the strains with respect to the maximum stamp displacement and bending temperature, the strain for first crack formation is determined. As this is a significant value, the critical strain ε_2 defines the lowest strain value where two cracks have already formed on the sample surface with an accuracy of 0.01%. This ensures the validity of this parameter.

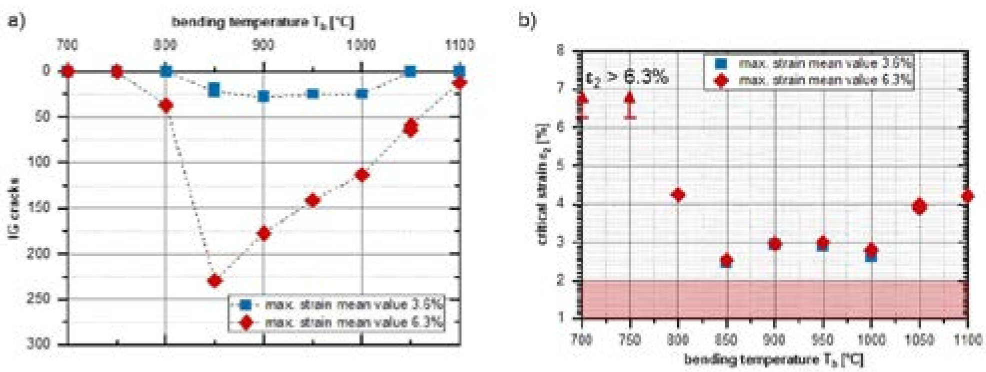

Fig.6 - a) Number of IG cracks for the whole temperature range and the two bending cases; b) Corresponding critical strain ε2 for all samples.

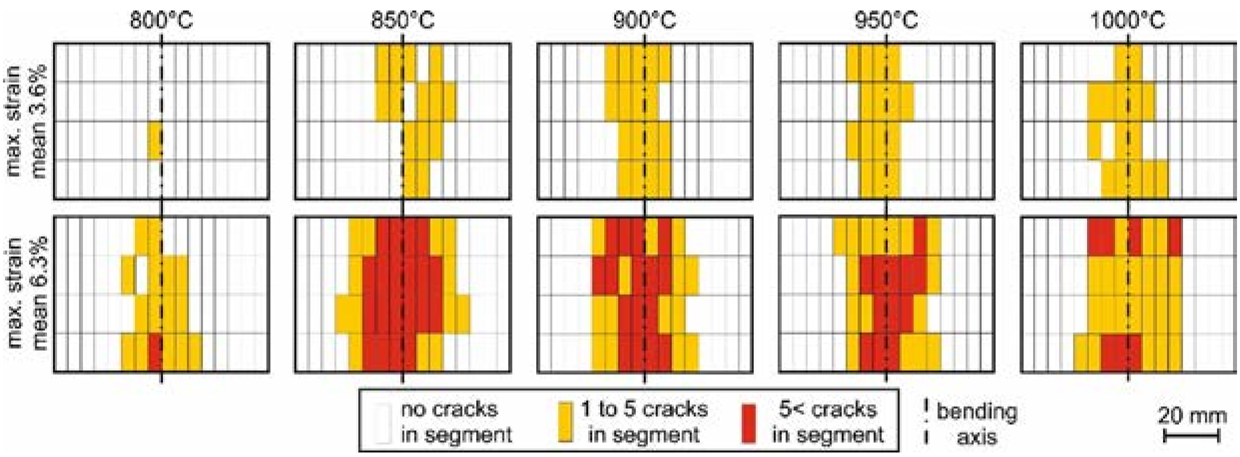

Fig.7 - Crack distributions T_b = 800°C, 850°C, 900°C, 950°C, 1000°C

The diagram in Fig. 6 b) presents the ε_2 values according to the samples in a). The noncritical temperatures 700°C and 750°C show no cracks, which means the value of ε_2 exceeds 6.3% and is therefore not relevant for conventional continuous casting. At 800°C, 1050°C and 1100°C the values of ε_2 range between 4.25% (800°C) and 3.88% (1050°C). This correlates to the samples with maximum strains of 3.6%, which show no cracks, as the critical strains exceed the maximum induced strain. The samples with the higher number of cracks at 850°C to 1000°C also reveal the lowest values of ε_2. At 900°C and 950°C all four values are nearly superimposable at 3%. At 850°C the most critical behavior, with ε_2 of 2.49%, is observed. The reproducibility at 850°C (max. strain 3.6%) and 1050°C (max. strain 6.3%) is again very accurate. Fig. 8 a) illustrates the number of cracks for samples with continuously increasing maximum strain at T_b = 900°C. For the validity of reproduction, every test is performed twice. The two samples with maximum strains below the critical strain limit don't reveal significant cracks on the surface. When that "barrier" is exceeded, the number of cracks increases with a nearly exponential progression. But the critical strain values in diagram b) confirm that the first crack formation doesn't depend significantly on the maximum induced strain. The mean value of critical strain is 2.95%, which is marked as the critical strain level. Fig. 9 shows crack distributions corresponding to diagram Fig. 8 b). The crack density increases with higher strains.

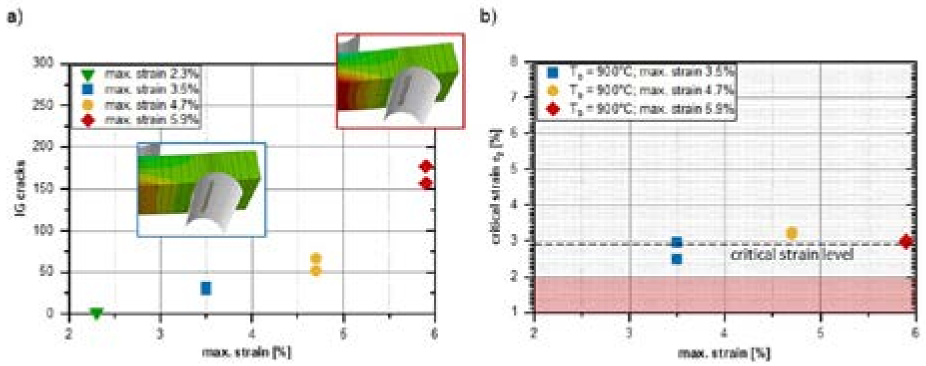

Fig.8 - a) Number of IG cracks for continuously rising maximum strains at T_b = 900°C; b) Corresponding critical strain ε_2 at T_b = 900°C.

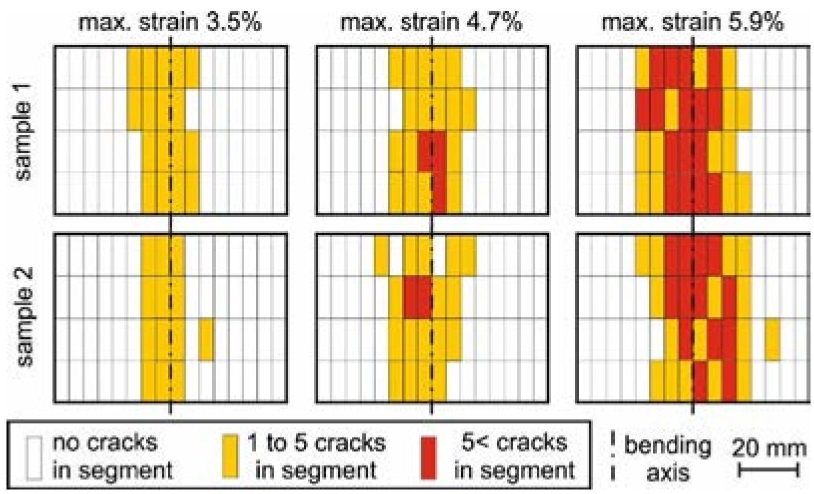

Fig.9 - Crack distributions T_b = 900°C, max. strain 3.5%; 4.7% and 5.9%.

DISCUSSION

Samples with differing maximum strains show dependency in the maximum strain and the number of cracks, but similarity in the critical strain ε_2. This points at certain strain-induced underlying mechanisms. More precisely, a high amount of deformation-induced AlN precipitates for the highest strains is plausible. Further on, these results indicate that for a steel composition with a certain set of testing parameters, the critical strain for first crack formation doesn't depend on the maximum induced strain. In fact, ε_2 represents a factor that shows the surface ductility of a current state dependent on the whole set of testing parameters. In addition, the highest maximum strain values enable the most detailed grading of results and provide more information of the material. The results permit an evaluation regarding surface cracking in the second ductility trough. Basically, the critical strains are higher than the mechanically induced strains in a conventional straightener (marked areas Fig. 6 b) and Fig 8 b)). In the case of the investigated steel grade and testing parameters, the risk of surface cracking is moderate, although the most critical temperature is 850°C. It should be kept in mind that the total strains on the strand surface can increase with additional thermal strain contributions or deep oscillation marks. The results are valid for the current testing parameters and steel composition. Changes in the parameters can, however, have a detrimental impact on the surface ductility; for example, less cooling in the mold, which leads to high temperatures of >1200°C for a certain time after the mold, can trigger pre-defects on the sample surface and bring about poor ductility in the critical temperature range; see Krobath et al. [23]. Therefore, it should be kept in mind that the testing conditions have to be as near as possible to the real casting process which is simulated, to reach the best goals in optimizing the process. Using the data of the IMC-B results for surface crack prediction models and calculations proves highly beneficial since a vast number of scenarios can be simulated to gain information for different mechanisms leading to surface cracks.

CONCLUSION

In the present study, the determination of the susceptibility to surface cracking in the range of the second ductility trough with the IMC-B test is exemplified. The most essential characteristics of the IMC-B test can be summed up as follows:

- Similar microstructure compared to the strand shell - directional dendrite growth and columnar austenite grains.
- Surface phenomena due to contact with atmosphere - no inert atmosphere in conventional IMC-B testing.
- Spectrum of strains and strain rates on the sample surface - information about the first crack formation.

The results of the evaluation of a 0.17 wt.% C steel are expressed with the number of cracks and the critical strain for crack formation. The most important results are:

- The most critical temperature range is revealed at 850°C to 1000°C.
- Noncritical behavior is observed at 700°C and 750°C.
- The lowest critical strain value of 2.49% shows the sample with a bending temperature of 850°C.

ACKNOWLEDGEMENTS

The authors gratefully acknowledge the funding support of K1-MET GmbH, metallurgical competence center. The research program of the K1-MET competence center is supported by COMET (Competence Center for Excellent Technologies), the Austrian program for competence centers. COMET is funded by the Federal Ministry for Climate Action, Environment, Energy, Mobility, Innovation and Technology, the Federal Ministry for Digital and Economic Affairs, the Federal States of Upper Austria, Tyrol and Styria as well as the Styrian Business Promotion Agency (SFG). Besides the public funding from COMET, this research project is partially financed by scientific partners and the industrial partners voestalpine Stahl and Primetals Technologies Austria.

REFERENCES

[1] Leitner R, Fuchshuber D, Brugger C, Pennerstorfer P. Digital Twin for continuous casters – the playground for metallurgists and process engineers. 4th European Steel Technology and Application Days. 2019 Jun 24-28; Dusseldorf, Germany. Steel Institute VDEh; 2019.

[2] Preuler L, Louhenkilpi S, Bernhard C, Ilie S, Taferner M. Utilization of Experimental Data as Boundary Conditions for the Solidification Model Tempsimu-3D. BHM 165; 2020; 5: 237-242.

[3] Brimacombe JK, Sorimachi K. Crack formation in the continuous casting of steel. Metall. Mater. Trans. B 8; 1977; 3: 489-505.

[4] Szekeres ES. A Review of Strand Castings Factors Affecting Transverse Cracks, 6th International Conference on Clean Steel. 2002 Jun 10-12; Balatonfüred, Hungary. OMBKE; 2002. p. 324-338.

[5] Xia G, Burgstaller K, Fürst C, Harrer B, Milosch E, Samoilov A. Influence of Steel Composition on Crack Formation on the Continuous Casting Steel Slab. 8th European Continuous Casting Conference. 2014 Jun 23-26; Graz, Austria. Leoben: ASMET; 2014, p. 729-739.

[6] Schwerdtfeger K. Crack susceptibility of steels in continuous casting and hot forming. Verlag Stahleisen GmbH: Dusseldorf, Germany, 1994.

[7] Crowther DN, Mintz B. Influence of Carbon on Hot Ductility of Steels. Mater. Sci. Tech. 2; 1986; 7: 671–676.

[8] Suzuki HG. Study of workability of continuous cast strand steels. PhD Thesis; Tohuku University; 1981.

[9] Abushosha R, Vipond R, Mintz B. Influence of sulphur and niobium on hot ductility of as cast steels. Mater. Sci. Tech. 7; 1991; 12: 1101–1107.

[10] Mintz B, Banerjee JR. Influence of C and Mn on hot ductility behavior of steel and its relationship to transverse cracking in continuous casting. Mater. Sci. Tech. 26; 2010; 5: 547–551.

[11] Mintz B, Crowther D.N. Hot ductility of steels and its relationship to the problem of transverse cracking in continuous casting. Int. Mater. Rev. 55; 2010; 3: 168–196.

[12] Revaux T, Deprez P, Bricout JP, Oudin J. In situ solidified hot tensile test and hot ductility of some plain carbon steels and microalloyed steels. ISIJ Int. 34; 1994; 6: 528-535.

[13] Schwerdtfeger K, Spitzer KH. Application of reduction of area-temperature diagrams to the prediction of surface crack formation in continuous casting of steel. ISIJ Int. 49; 2009; 4: 512-520.

[14] Crowther DN. The Effects of Microalloying Elements on Cracking During Continuous Casting. The Use of Vanadium in Steel - Vanitec Symposium. 2001; Bejing, China.

[15] Schmidt F, Gross O. The Continuous Casting of Small Sections. Steel Int. 3; 1967; 1: 11-23.

[16] Lankford WT. Some Considerations of Strength and Ductility in the Continuous Casting Process. Metall. Trans. 3; 1972; 6: 1331-1357.

[17] Burden MH, Funnel GD, Whitaker AG, Young JM. Origins of defects in continuously cast blooms produced on a curved mould machine. Solidification and Casting of Metals. 1979; London; UK; p. 279–286.

[18] Yasumoto K, Maehara Y, Nagamichi T, Tomono H. Effect of Thermo-Mechanical History on Surface Cracking of As-Cast Low Carbon Low Alloy Steel Slabs. Tetsu to Hagane 73; 1989; 10: 1381–1388.

[19] Crowther DN, Green MJW, Mitchell PS. The influence of composition on the hot cracking susceptibility during casting of microalloyed steels processed to simulate thin slab casting conditions. Mater. Sci. Forum 284-286; 1998; 469-476.

[20] Krobath R, Bernhard C, Ilie S, Six J, Hahn S, Pennerstorfer P. A new method for the experimental simulation of surface crack formation in continuous casting. La Metallurgia Italiana 5; 2017; 4: 5–13.

[21] Krobath R, Bernhard C. A New Experimental Setup for the Simulation of Surface Crack Formation in the Continuous Casting Process. AISTech. 2017 May 8-11; Nashville, TN, USA. Association for Iron & Steel Technology; p. 1827–1837.

[22] Krobath R, Bernhard C, Ilie S, Six J, Hahn S, Pennerstorfer P. The role of grain boundary oxidation on surface crack formation under continuous casting conditions. BHM 164; 2019; 11: 461-465.

[23] Krobath M, Krobath R, Bernhard C, Ecker W. Elasto-Viscoplastic Material Model of a Directly-Cast Low-Carbon Steel at High Temperatures. Materials 13; 2020; 2281.

[24] Presslinger H, Mayr M, Tragl E, Bernhard C. Assessment of the Primary Structure of Slabs and the Influence on Hot- and Cold-Rolled Strip Structure. Steel Res. Int. 77; 2006; 2: 107-115.

[25] Reiter J, Bernhard C, Presslinger H. Austenite grain size in the continuous casting process: Metallographic methods and evaluation. Mater. Charact. 59; 2008; 737-746.

[26] Ohno M, Tsuchiya S, K. Matsuura. Microstructural Features and Formation Processes of As-cast Austenite Grain Structures in Hypoperitectic Carbon Steels. ISIJ Int. 55; 2015; 11: 2374–2382.

[27] Krajewski P, Krobath R, Bernhard C, Miettinen J, Louhenkilpi S, Ilie S, Schaden T. A Novel Approach for the Simulation of Surface Crack Formation in Continuous Casting. BHM 160; 2015; 3: 109–116.

[28] Zhang X, Zhu H, Huang W, Shi B, Tieu AK. Investigation on slab continuous straightening technology and deformation analysis. Int. J. Mater. Prod. Tec. 47; 2013; 126-137.

[29] Suzuki M, Hayashi H, Shibala H, Toshihiko E, In-Jae L. Simulation of transverse crack formation on continuously cast peritectic medium carbon steel slabs. Steel Res. 70; 1999; 10: 412-419.

[30] Bernhard C, Pierer R, Tubikanec A, Chimani C. Experimental characterization of crack sensitivity under continuous casting conditions. Continuous Casting and Hot Rolling Conference. 2004; Linz; Austria.

[31] Ilie S, Reiter J, Presslinger H, Fluch J, Bernhard C. Characterization of hot tear segregations in continuous casting of slabs. 6th European Continuous Casting Conference. 2008 Jun 3-6; Riccione, Italy.